Light-Emitting Organic Semiconductor-Incorporated Perovskites: Fundamental Properties and Device Applications

Wenhao Shao[†], *Seokjoo Yang*[†], *Kang Wang*[†], *Letian Dou*[*,†]

[†]Davidson School of Chemical Engineering, Purdue University, West Lafayette, IN, USA.

[*]E-mail: dou10@purdue.edu

ABSTRACT

Recently, organic semiconductor-incorporated perovskites (OSiPs) have emerged as a new subclass of the next-generation organic-inorganic hybrid materials. OSiPs combine the advantages of organic semiconductors, such as large design windows and tunable optoelectronic functionalities, with the excellent charge-transport properties of the inorganic metal-halide counterparts. OSiPs provide a new materials platform for the exploitation of charge and lattice dynamics at the organic-inorganic interfaces for various applications. This perspective article reviews recent achievements in OSiPs highlighting the benefits from organic semiconductor incorporation and elucidates the fundamental light-emitting mechanism, energy transfer, as well as band alignment structures at the organic-inorganic interface. Insights on the emission tunability are led towards a discussion on the potential of OSiPs in light-emitting applications such as perovskite light-emitting diodes or lasing systems.

TOC Graphic

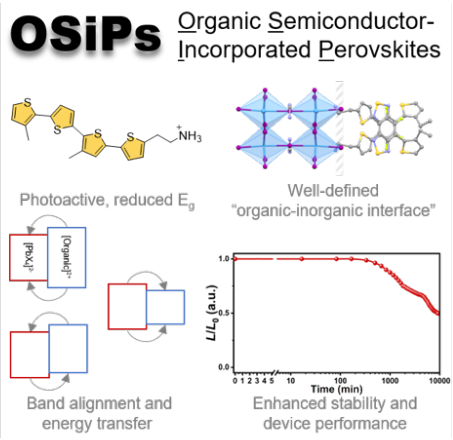

Metal-halide perovskites are promising materials for the next generation displays,[1–4] photovoltaics,[5–7] and radiation detection platforms[8–11] due to their advantageous solution processability, carrier transporting efficiencies, and defect tolerance.[12] The unique crystal structure of metal-halide perovskites has inspired exploration on the functional interface between inorganic lattices and organic building blocks, and thus led to a recent novel class of "Organic Semiconductor-Incorporated Perovskites" (OSiPs).[13,14] OSiPs exploit the advantages of organic semiconductors in these hybrid materials such as their large design windows, enhanced carrier mobility, and tunable frontier molecular orbitals to aligns with the perovskite counterparts.

The crystal lattice of metal-halide perovskites consists of corner-sharing metal-halide octahedrons stabilized by organic ammonium cations: in 3D perovskites having the general formula of ABX_3 with B as the metal cation (Pb or Sn) and X as halides (Cl, Br, or I), A site cations are usually small-size organic methylammonium (MA), formamidinium (FA) or inorganic Cs. Although the choice of A site cations is limited, the grain boundaries of 3D perovskites could accommodate additional functional cations for defect passivation or grain-size control.

3D halide perovskites could be further reduced to 2D and lower dimensional structures with the incorporation of bulkier organic cations/ligands, commonly referred to as LA. The widely explored Ruddlesden-Popper (RP) phase features the layered structures with the general formula of $LA_2A_{n-1}B_nX_{3n+1}$ where a number (n) of inorganic layers are sandwiched between structure-directing LAs, forming a characteristic multiple quantum-well (MQW) structure. As the size restriction is lifted in reduced-dimension perovskites, bulky organic semiconducting ligands with sophisticated structures and functionalities could be incorporated into the crystal lattices rather than merely at the grain boundaries.

This perspective aims at drawing widespread attention to the benefits that organic semiconductors could bring to metal-halide perovskites with a special focus on the emission tunability of OSiPs and light-emission applications. We start from reviewing the recent progress in the OSiP regime to highlight the advantages of organic semiconductor incorporation. As the energy gap of organic semiconductors are largely reduced compared to insulating LA cations, the band alignment at the organic-inorganic interface and the resulted interfacial energy transfer (ET) mechanism needs to be well-elucidated and hence will be addressed extensively in this article. Afterwards, state-of-the-art light-emitting applications highlighting the potential of organic semiconducting ligands will be discussed. Our own understanding and perspectives on challenges

and future research directions are embedded at the end of each section to inspire next-generation researchers in this rapidly growing field.

Advantages of Organic Semiconducting Cations

Figure 1 summaries the key structural features and advantages of OSiPs over conventional layered halide perovskite materials. Some of the key properties are briefly discussed in this section.

Enhanced carrier mobility and conductivity. One great advantage of organic semiconductors over insulating cations is their enhanced carrier mobility due to higher dielectric constants in conjugated systems. Despite the extraordinary in-plane conductivity in the metal-halide slabs, the out-of-plane carrier mobility of 2D layered perovskites are significantly limited by LA cations with wide energy gaps. In this regard, conjugated arene have been designed as LA s and exhibited enhanced out-of-plane conductivity to 10^{-4} S/m, which is orders of magnitude higher than that when aliphatic LAs were used.[15]

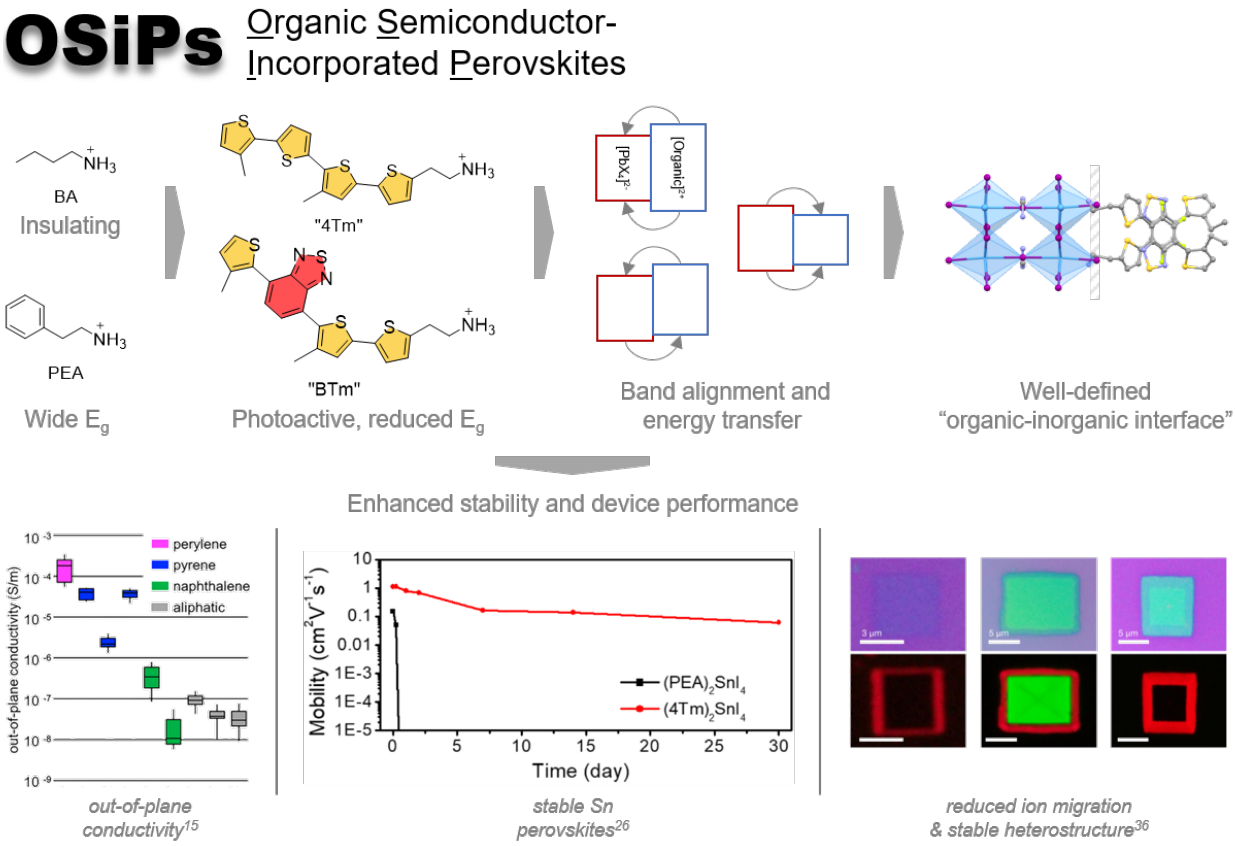

Figure 1. A summary of key structural features and advantages of OSiPs. (bottom left) Reproduced with permission from ref 15. Copyright 2018 American Chemical Society. (bottom mid) Reproduced with permission from ref 26. Copyright 2019 American Chemical Society. (bottom right) Reproduced with permission from ref 36. Copyright 2020 Springer Nature.

Another important consideration of organic semiconducting cations is the tunability of their energy gap and frontier molecular orbitals, namely the highest occupied and lowest unoccupied molecular orbitals (HOMOs and LUMOs, respectively). The HOMO and LUMO energy levels of organic semiconductors could be brought close to the valence band (VB) and conduction band (CB) of metal-halide layers, respectively, resulting in improved charge injection into the perovskites as well as charge extraction.

This idea has been exploited by incorporating oligothiophene based cations as passivators for the surface defects in 3D perovskite solar cells.[16] While most surface passivation techniques introduce insulating small molecules to the interface between 3D perovskites and carrier transporting layers, they inevitably created an additional barrier hindering charge transport. Recently, a monoammonium conjugated cation named 4Tm has been developed based on modified quaterthiophene derivative envisioned by Mitzi *et al.* back in 1999.[17] With a facile post-fabrication treatment, 4Tm halide salts could be anchored on the surface of 3D lead iodide perovskites to form 2D perovskites *in situ* with a Type II band alignment to assist hole extraction. Enhancement in hole mobility, reduced interface recombination rate, and improved power conversion efficiency (PCE) from 19.9% to 22.0% were observed.[16]

High carrier mobility in organic semiconducting passivators is meaningful as well in perovskite quantum dot (PQD) based light-emitting applications where a large content of surface capping ligand is needed considering the nm-sized PQDs. Consequently, carrier mobility in the capping ligands as well as inter-PQD electronic coupling need to be considered for the overall conductivity of the films. To this end, recent progress pointed to the efficient inter-PQD electronic interaction through ligand-ligand π-π interactions.[18]

Environmental stability. Metal-halide perovskites are susceptible to degradation induced by light, moisture, or oxygen.[19] Compared to 3D perovskites, 2D layered structures have reduced surface energy, higher formation energy, and intrinsic LAs to passivate their surfaces against environmental damage.[20] However, this shielding effect from small organic cations are limited, which is particularly significant for Sn based perovskites that suffer from intrinsic poor stability due to the easy oxidation from Sn(II) to Sn(IV).[21,22] More importantly, the potential of Sn-based perovskites is similar to or in some cases even higher than their Pb counterparts.[23] For instance, $MASnI_3$ single crystals have extremely high carrier mobility of up to 2,000 $cm^2V^{-1}s^{-1}$;[24] the low

thermal conductivity of Sn-based perovskites also makes them suitable for thermoelectric devices.[25]

These characteristics imply the need for bulkier and more hydrophobic organic cations, which makes organic semiconductors competent candidates. Recently, 4Tm as LAs has been introduced to Sn-based perovskite field-effect transistors (FETs) which led to highly stable performances over several days compared to when small phenyl-ethylammonium (PEA) cations were employed.[26] This, together with the higher carrier mobility and hole conductivity of 4Tm cations, resulted in enhanced hole mobility up to 2.32 $cm^2V^{-1}s^{-1}$. Similar strategies have been applied to stable LEDs with operational stability over 150 h.[27]

Reduced ion migration and accessible heterostructures. The crystal lattice of metal-halide perovskites is considered soft and tolerant to defects, but this also facilitates ion diffusion predominantly through lattice distortion and structural defect sites.[28] Consequently, hysteresis behavior[29] and electrical poling effects[30] are typically observed under device operation, reducing their operation lifetime and performance stability. Among the ionic species in perovskite lattices, halides have the lowest diffusion energy barrier compared with metal cations and organic cations, either A site cations or bulkier LAs.[28] In 2D perovskites with layered structures, ion diffusion happens both along the lateral direction (i.e. within the perovskite layer)[31,32] and vertically through the organic wells[33,34]. With the incorporation of bulkier organic semiconducting LAs with rigid backbone, it was observed that both vertical and lateral halide migration could be suppressed,[28] which could lead to enhanced operational stability when bias is applied.

Reduced ion migration with organic semiconducting LAs has also been translated to accessible and stable vertical or lateral heterostructures based on 2D perovskites with sharp junction width and enhanced thermal stability.[35,36] These platforms further inspired fundamental studies on the halide diffusion mechanism and kinetics through tracking the structural and compositional change across the heterostructure junctions.[31,33] It has been recently discovered through these systems that halide diffusion through vertical heterostructures across bulkier organic layers follows a unique "quantized" layer-by-layer mechanism largely depending on the shielding effects of cations, which is distinct to the classic and more efficient concentration driven diffusion along the lateral direction.[33] In addition, since organic cations become optically active due to their significantly reduced energy gaps, exciton interactions at the interface of 2D perovskite heterostructures, such

as the formation of charge-transfer excitons[37] or interlayer excitons in general, could be studied in a more systematic manner under various band-alignment structures.

The above-mentioned advantages make OSiPs interesting for fundamental materials chemistry and physics studies, as well as promising for a variety of device applications. Particularly, OSiPs are exciting for light-emitting applications because of their intrinsic quantum well structures, tunable band gap and exciton properties, and enhanced stability. In the following part of this article, we mainly focus on their optical properties and associated optoelectronic and photonic applications.

Unique Optical and Optoelectronic Properties of OSiPs

In OSiPs where organic semiconducting cations carry functional responsibilities, band alignment at the organic-inorganic interface predominantly determines the macroscopic charge carrier behaviors and optoelectronic properties. In this regard, 2D perovskites featuring MQW structures, close organic-inorganic interaction, and well-defined interface are ideal systems to discuss the band alignment, energy and charge transfer at the organic-inorganic interface. Before moving forward, the fundamental band structure and dissimilarity between organic and inorganic semiconductors needs to be elucidated.

Band alignment and energy transfer fundamentals in 2D MQW structures. Metal-halide perovskites and inorganic semiconductors generally display continuous CB and VB consist of the combination of orbitals close in energy. The VB of hybrid lead-halide perovskites, for instance, consist mostly of halide frontier *p* orbitals with some lead 6*s* characters, while their CB dominated by lead 6*p* bands.[38] In contrast to 3D perovskites, the exciton binding energy in 2D perovskites is considerable (E_b>300 meV)[39] and thus excitons are formed spontaneously below the CB minimum upon photo-excitation and participate in the ET at organic-inorganic interfaces (Figure 2A, left). On the contrary, due to the lower dielectric constants and their weak intermolecular electronic coupling, organic semiconductors display discrete energy levels with their photophysical and optoelectronic characteristics largely determined by HOMOs, LUMOs, and nearest few frontier molecular orbitals (e.g. HOMO-1, LUMO+1, etc.). (Figure 2A, right) In addition, the low dielectric constants in organic semiconductors lead to the formation of distinct singlet and triplet excitons with even higher E_b (as high as 1.5 eV).[40] As a result, the lowest singlet and triplet states (S_1 and T_1, respectively) are deeply inserted into the energy gap.

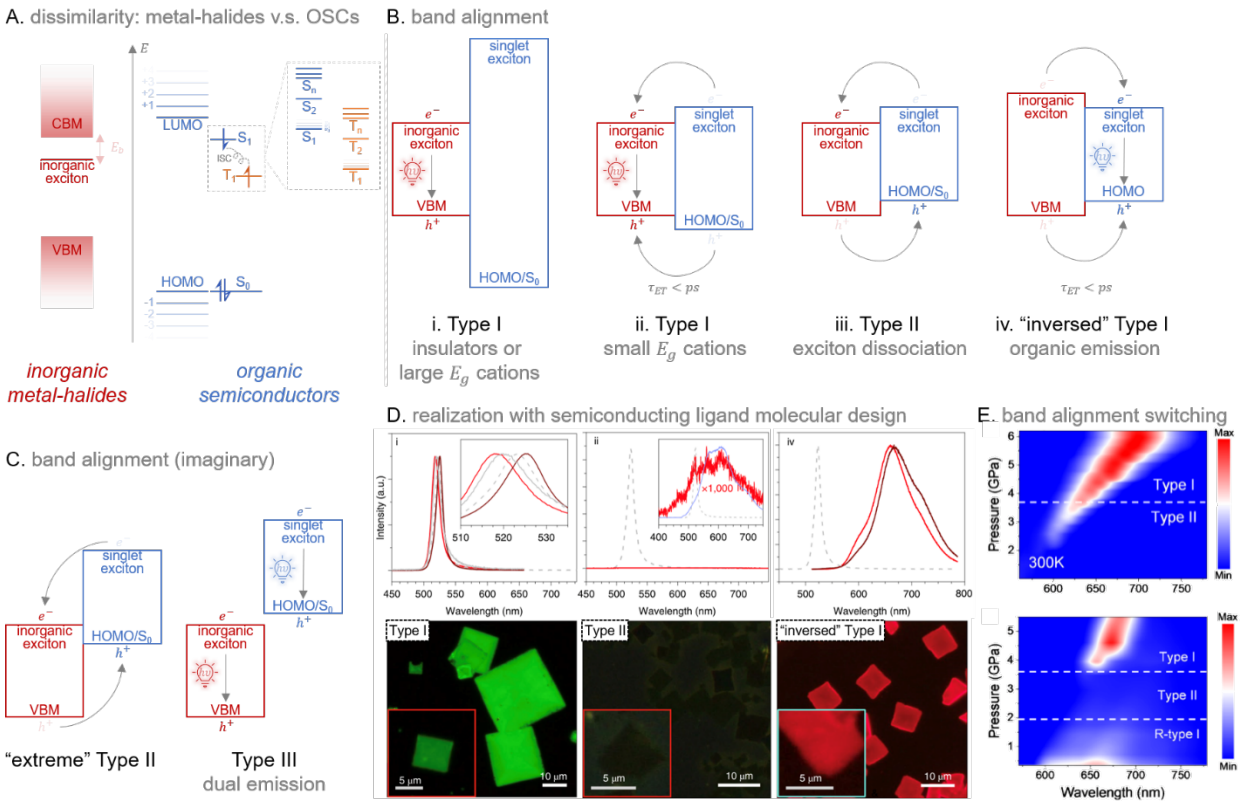

Figure 2. Band alignment and energy transfer fundamentals in 2D OSiPs. (A) energy and band diagrams of inorganic metal-halides and organic semiconductors showing their dissimilarities: the former feature continuous bands while the latter have discrete energy levels due to weak intermolecular interactions. The singlet and triplet levels of organic semiconductors are shown as well. Archetypical band alignment structures between PVSKs and organic semiconductors are shown in (B), which was extended to a few imaginary cases in (C). (D) Recent realization of versatile band alignments with careful molecular design of organic semiconductors. Reproduced with permission from ref 41. Copyright 2019 Springer Nature. (E) Band alignment switching in response to pressure. Reproduced with permission from ref 42. Copyright 2022 AAAS.

Due to the dissimilarity between organic and metal-halide layers, energy and charge transfer between these two entities and their band alignment needs to be cautiously discussed to account for the interactions between inorganic excitons, organic singlet, and triplet excitons. Direct photo-excitation normally yields negligible triplet excitons due to their low transition dipole moment, and hence photo-generated triplet excitons rely on intersystem crossing (ISC) from singlet excitons, the mechanism of which depends on the spin-orbit coupling (SOC) between the orbitals involved.[43] SOC constant is typical low in light elements-dominated organic semiconductors and hence singlet excitons are generally considered when discussing the interfacial ET in 2D quantum

well PVSKs. Hence, the band alignment at the interface is usually simplified to involve inorganic VBM, inorganic exciton level, the organic HOMO, and S_1. (Figure 2A)

While photo-excitation leads to fast formation of excitons, uncorrelated electrons and holes are injected into PVSKs in devices and thus charge transfer needs to be elucidated besides exciton-mediated energy transfer. For instance, electron injection from organic LUMO to metal-halide could compete with organic exciton formation. Our further discussion on this matter is limited by the literature support and thus primarily focused on photo-excitation and ET.

Conventionally when insulating or less-conjugated LAs are employed, Type I alignment at the organic-inorganic interface is expected with the HOMO and S_1 of organic LAs deeply inserted into the VB and CB of inorganic metal-halide layers, respectively (Figure 2B-i). When organic semiconducting LAs with reduced energy gaps are incorporated, more efficient sub-ps ET could be achieved due to increased exciton wavefunction overlap at the interface (Figure 2B-ii).[27] Accordingly, high-lying excited states in organic semiconductors could participate in ET if energetically aligned with inorganic excitons, since this ultrafast ET is able to outcompete the exciton relaxation processes from higher-energy states to S_1[44] or the formation of ICT states.[27]

On a broader scope, the tunability of interfacial band alignment and subsequent light emission extend well-beyond traditional Type I with organic-to-inorganic ET. Type-II alignment allows the fast separation of bounded electrons and holes at the interface (within 10 ps, Figure 2B-iii),[41] making organic semiconductors promising multifunctional passivators for 3D perovskites to enhance carrier extraction efficiency.[16] On the other hand when incorporating organic semiconductors with further reduced energy gaps, ET from metal-halide slabs to organic wells could be anticipated in "inverted" Type-I systems (Figure 2B-iv). As discussed later, they have become prominent platforms to explore the photophysics of organic semiconductors in the perovskite matrices. As expected, sub-ps fast ET has also been observed in these structures.[41]

In addition, although its practical value has not been reported, Type-III or extreme Type-II alignments are theoretically plausible if the interfacial band overlap is eliminated and thus energy transfer is restricted (Figure 2C). This could be done by introducing strongly electron donating or accepting LAs or by using quasi-2D perovskites to reduce the inorganic band gap. These systems could potentially produce spontaneous charge transfer and / or white emission as a combination of both organic and inorganic luminescence.

Recent progresses have seen the energy level fine-tuning capability of organic semiconducting LAs in 2D OSiPs to meet the aforementioned band alignments with the benchmark oligothiophene derivatives (Figure 2D).[41] This, combined with the reduced ion migration, has made OSiPs suitable platforms to create a wide-range of colorful lateral and vertical heterostructures with tailor-designed band alignment across the sharp heterostructure junction.[36] Furthermore, the band alignment at the organic-inorganic interface could be subject to shift in response to external stimuli, either through introducing photoswitchable organic cations[45] or by engineering the soft lattice of metal-halide layer. For instance, pressure has been demonstrated as a facile tool to induce faster variation on the inorganic bang gap (~100 meV/GPa) compared to the energy gap variation in the organic well. The interfacial band alignment could be switched from Type I to II and even to inversed Type I (Figure 2E) upon applying external pressure, which could be used to fine-tune the band-edge state and charge-distribution at the organic-inorganic interface.[42] This "pressure gate" strategy could be meaningful for futuristic optical switches and modulators.

In summary, perovskites now possess functional and engineerable organic-inorganic interfaces and expanded tunability on their optoelectronic properties, both of which are activated by the incorporation of organic semiconductors with tunable structures and sophisticated functionalities.

Harvesting organic triplet excitons in 2D quantum well PVSKs. Although light-element dominated organic semiconductors typically possess low SOC constants and ISC efficiency, interestingly in inverted Type-I structures, ET from metal-halides is able to bypass the singlet states and directly access organic triplet states.[46] This mechanism requires close wavefunction overlap between organic triplet excitons and inorganic excitons and simultaneously high-lying organic S_1 states, which is accessible in wide gap organic semiconductors possessing large singlet-triplet energy gap (ΔE_{ST}). (Figure 3A) In reality, enhanced organic phosphorescence has been observed by Era *et al.* in 1998[47] using naphthalene-based LAs in 2D Pb-Br PVSKs. The ET mechanism has been elucidated later by Ema *et al.* in 2008[46] which revealed a Dexter-type ET (DET) route from the inorganic triplet excitons to organic triplet excitons driven by their wavefunction overlap. (Figure 3A) In detail, the rich vibrational levels of the naphthalene T_1 state efficiently intakes energy from inorganic excitons. Once triplet excitons are formed from DET, they quickly relaxed to the lowest vibrational state within picosecond and thus back energy transfer could be prevented. The DET constant (τ_{ET}) is exponentially dependent on the distance between

$[PbBr_4]^{2-}$ slabs and the naphthalene core. When the distance was reduced to ~1 Å, τ_{ET} could be boosted below 30 ps^{-1} and the DET efficiency (η_{ET}) above 99%. (Figure 3A)

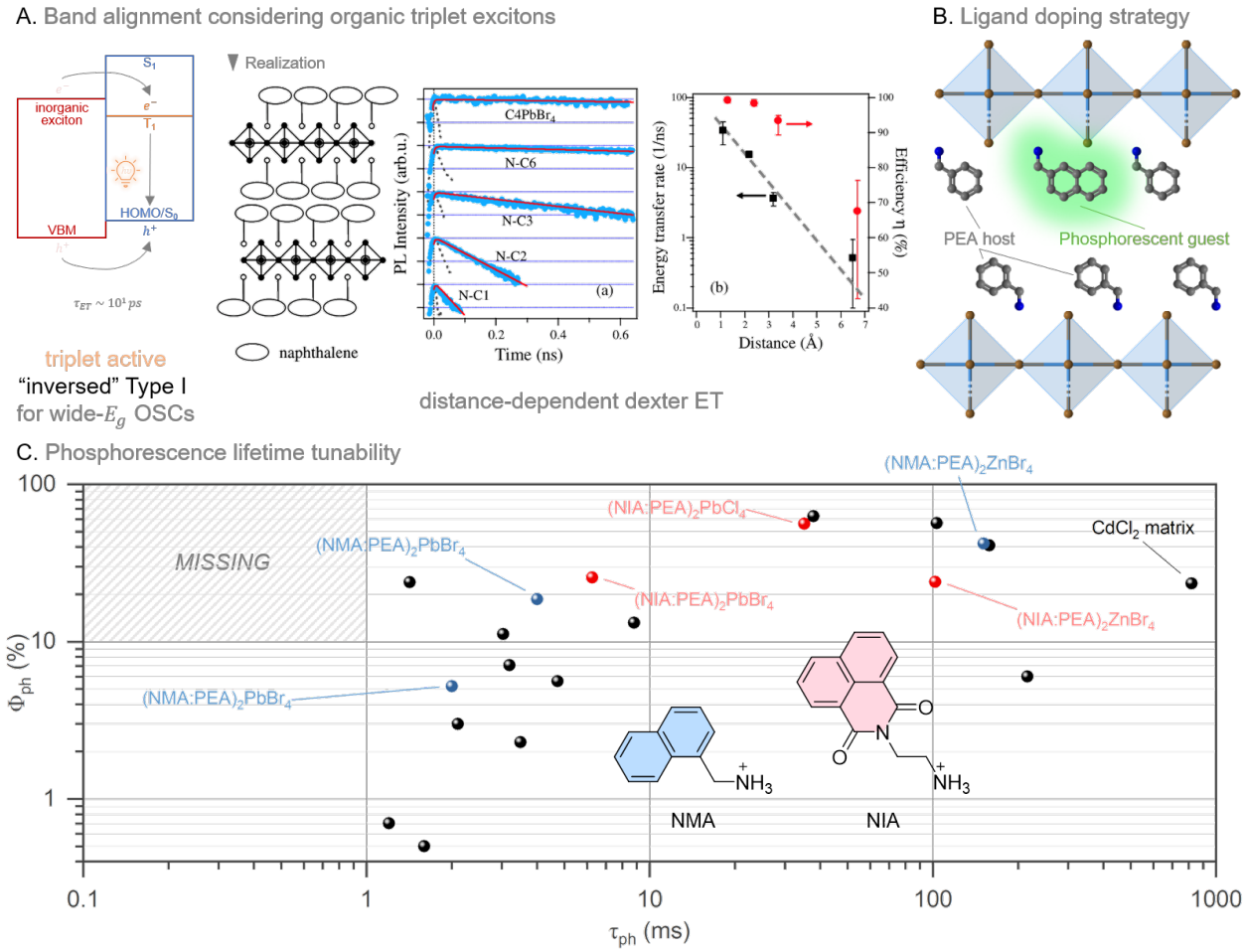

Figure 3. Contemporary strategies to harvest organic triplet excitons in 2D OSiPs, which relies on direct energy transfer from inorganic excitons to organic triplet excitons (**A**) and could bypass low ISC yield in conventional organic semiconductors due to their high-lying singlet states. This efficient energy transfer is via the dexter pathway (**A**, right). Reproduced with permission from ref 46. Copyright 2008 American Physical Society. (**B**) Efficient organic phosphorescence could be achieved by doping phosphorescence **LAs** in optically inert counterparts (e.g. PEA). (**C**) Summary on the lifetime tunability and quantum yield of contemporary organic phosphorescent systems using perovskite as energy donor and host. Material systems based on naphthalene methylammonium (NMA) and naphthalene imide ethylammonium (NIA) **LAs** are highlighted.

2D PVSKs have been further demonstrated as advantageous matrices to induce highly efficient organic room-temperature phosphorescence (RTP). On one hand, the efficient interfacial DET could bypass the usually low ISC yield in organic semiconductors. On the other hand, the crystalline perovskite matrix and well-ordered long-range LA packing conformation are able to suppress the intermolecular collision-driven non-radiative decay for organic triplet excitons.[48]

Highly efficient organic RTP with phosphorescence quantum yield (Φ_{ph}) over 10% has been demonstrated by doping energetically suitable (i.e. sub-gap organic T_1 and high-lying S_1) phosphorescent cations into wide-gap optically inert LAs like PEA,[49,50] which resulted from reduced exciton annihilation and aggregation caused quenching – commonly observed in densely packed chromophores (Figure 3B).[51] The doping strategy also allows the incorporation of bulkier organic semiconducting cations and shorter alkyl ammonium chains to reduce the distance between phosphorescent cores and metal-halide slabs for efficient DET.

Lifetime tunability of organic RTP could be achieved using 2D perovskite matrices through the choice of metal and halide elements and the subsequent external heavy atom effect. In detail, SOC of phosphorescent LAs is sensitive to the atomic size of elements in the inorganic layer through their electronic interference in the molecular orbitals of LAs.[43,52] By replacing Br with lighter Cl, the RTP lifetime (τ_{ph}) could be elongated from 10^0 to 10^2 ms.[49] Figure 3C summarized the τ_{ph} and Φ_{ph} of organic RTP systems using 2D perovskite as host systems based on the recently published review.[48] Further reducing the phosphorescence decay rate is achievable by replacing heavy Pb and exploring other lead-free metal halide structures, such as zinc[53] or cadmium[54] based 2D structures. These strategies enable lifetime tunability of organic RTP from 2D OSiPs and hybrid metal-halide structures in the range of 10^0 ms to 1 s, while maintaining efficient Φ_{ph} over 10%.[48]

However, current exploration on phosphorescent organic cations isn't sufficient to push their RTP lifetime below the ms regime, which is crucial for their display applications where long-lived triplet excitons may induce device efficiency roll-off due to various exciton annihilation processes.[55] This is because of the limited internal SOC of phosphorescent cations currently employed in perovskites. Recently, various molecular design strategies have been proposed to enhance the internal SOC of metal-free covalently bonded organic phosphors by exploring the El-Sayed rule and introducing halogen[56] or chalcogen[57] heavy atoms, as well as exploiting the synergetic relationship of these two effects, realizing intrinsic phosphorescent lifetime as low as 100 μs.[52,58] Triplet excitons were also harvested by means of thermally-activated delayed fluorescence (TADF) through a small ΔE_{ST} and the subsequent efficient reverse ISC channel,[59] which has led to even faster delayed emission with τ_{ph} below the 10^1 μs regime and highly efficient organic LEDs (OLEDs) with external quantum efficiencies (EQE) approaching 40%.[60–62] Incorporating these triplet emitting molecules as perovskite cations could potentially utilize the

external heavy atom effects from lead-halide slabs to further reduce their delayed emission lifetime and thus creating new hybrid display systems combining the solution processability of perovskite materials with the stability and large design window of organic semiconductors.

Light Emitting Applications of OSiPs

Perovskite light-emitting diodes (PeLED). PeLED employs organic cations as passivators for 3D perovskites or as structural directing and functional LAs in quasi-2D structures. Conventionally, small insulating organic cations could be attached to 3D perovskites to achieve decreased surface defect density due to the in-situ formation of 2D perovskites (Figure 4A).[1] Molecular design descriptors for passivators have implied the need for sophisticated conjugated units back in 2018,[63] where the effect of alkyl ammonium anchoring tail length, aromatic units, and fluorination were explored (Figure 4B). Long alkyl chain decreases the photoluminescence quantum yield (PLQY) of passivated 3D perovskites because of the surface steric hinderance that restricts a dense passivation (Figure 4C). Also, cations having phenyl moieties induced higher PLQY than aliphatic derivatives, while fluorinated passivators also led to enhanced PLQY due to the greater vacancy formation energy inherited from the high electronegativity of fluorine. Subsequently, various fluorinated passivating cations have been developed in more recent studies.[64,65]

Recently, a series of semiconducting aromatic moieties were studied in perovskite passivators with expanded anchoring units.[66] As combining phenyl and thiophene cores with anchoring tails of MA, FA and imidazolium (Im), six novel molecular passivators were devised and applied to $MAPbI_3$-based PeLEDs (Figure 4D). The current density is similar for all samples with negligible leakage current below 2 V, however, the effect of cation passivation is clearly shown in radiance because passivators can reduce non-radiative recombination (Figure 4E). Finally, compared with thiophene-based cations, the phenyl core structure rendered devices with higher EQE, and the passivation effect of the anchoring tails is revealed in the order of Im, MA and FA (Figure 4F). Although these studies show that the conjugated derivatives can passivate defects, the benefits of semiconducting nature of the conjugated cation design were not fully demonstrated.

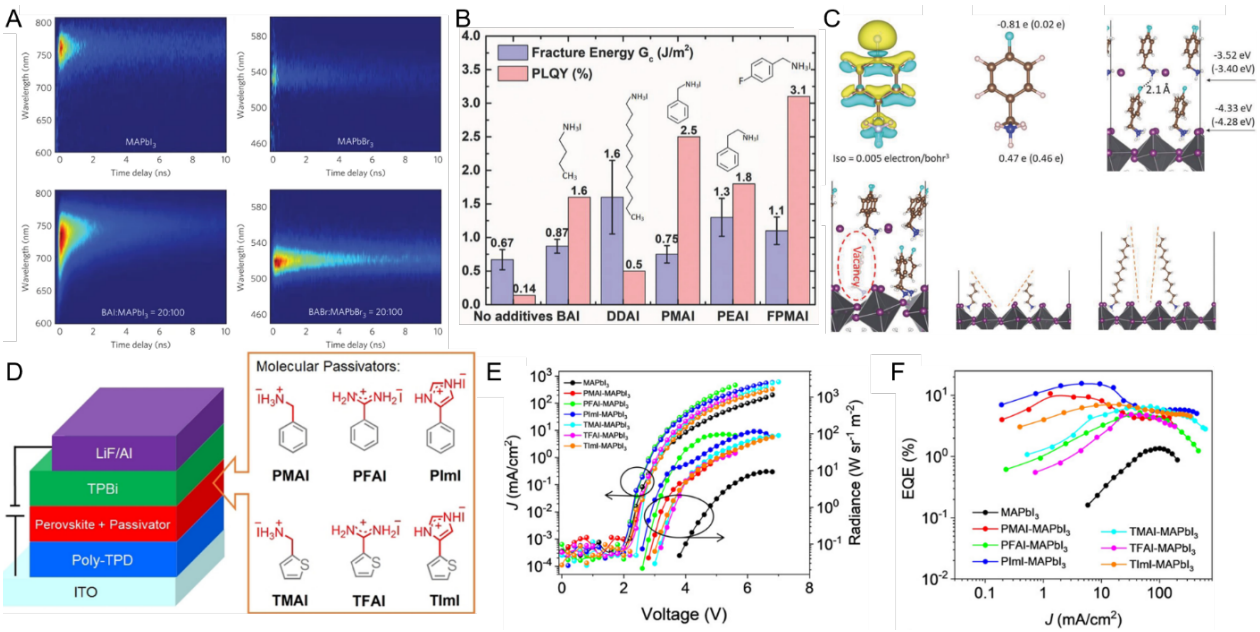

Figure 4. Passivating organic cations for 3D perovskites: towards sophisticated semiconducting moieties. (A) Time-resolved PL spectra of $MAPbI_3$ perovskite films without (top) and with (bottom) butylammonium (BA) cations as passivators.[1] (B) PLQY of perovskite films with various passivating organic cations.[63] (C) Calculations for vacancy formation energy of fluorination effect and schematic diagrams for interface between passivating cations and perovskites.[63] (D) Device architecture of a perovskite LED and molecular structure for various organic semiconducting passivators as well as (E) current density-voltage-luminescence and (F) EQE characteristic of the perovskite LEDs with these passivators.[66] (A) Reproduced with permission from ref 1. Copyright 2017 Springer Nature. (B-C) Reproduced with permission from ref 63. Copyright 2018 Wiley. (D-F) Reproduced with permission from ref 66. Copyright 2021 Wiley.

In quasi-2D PeLED, dimensionality defined as "*n* phase", thickness of inorganic layers, can show a variety of luminescent properties due to the quantum confinement effect. However, control of *n* phase is a crucial issue because of undesired multi-*n* phase formation in quasi-2D perovskite layers. The inhomogeneity of *n* phase in quasi-2D perovskite films can induce low EQE and multiple emissive species in PeLED devices. In this regard, bulky conjugated LA cations are found to have additional benefits in terms of modulating thin film growth and regulating *n*-phase distribution. Conventionally, modified PEA derivatives were studied extensively as LAs in quasi-2D PeLEDs. For example, naphthalene-based NMA and phenyl-butylammonium (PBA) have recently been studied as promising candidates. Quasi-2D PeLEDs using NMA as LA cations displayed high EQE over 20%.[3,67–71] In another example, the emission wavelength of quasi-2D PeLED can be well-controlled with PBA cations.[4,72–76] In addition, narrow phase distributions and reduced Auger recombination were observed in quasi-2D PeLED by incorporating fluorinated

PEA cations and inserting oxygen into their molecular backbone.[77,78] Although fluorine was attached to the organic cation, its electron-withdrawing characteristics rendered a 150 meV reduction in the E_b perovskites, which is proportional to the rate of Auger recombination. E_b could also be engineered by insertion of non-cation accepting molecules into the Van der Waals gap.[79] These studies imply the need for more sophisticated cation design and functional group attachment to control the excitonic behavior of perovskites in PeLEDs.

Very recently, Wang *et al*. designed a series of novel semiconducting LA cations featuring twisted bi-phenyl moieties with enhanced cross-section area and bulkiness. These derivatives were found to effectively regulate *n* phase separation by suppressing ion migration.[80] As a result, small *n* phase of 1 or 2 and high *n* phase of over 8 were almost eliminated (Figure 5A-B). Suppressed ion migration and *n* phase separation lead to high EQE over 26% at a peak wavelength of 700 nm and enhanced operational stability. Utilizing bulky organic semiconductors to regulate the formation of quasi-2D perovskites should be an effective mean towards highly efficient quasi-2D PeLEDs.

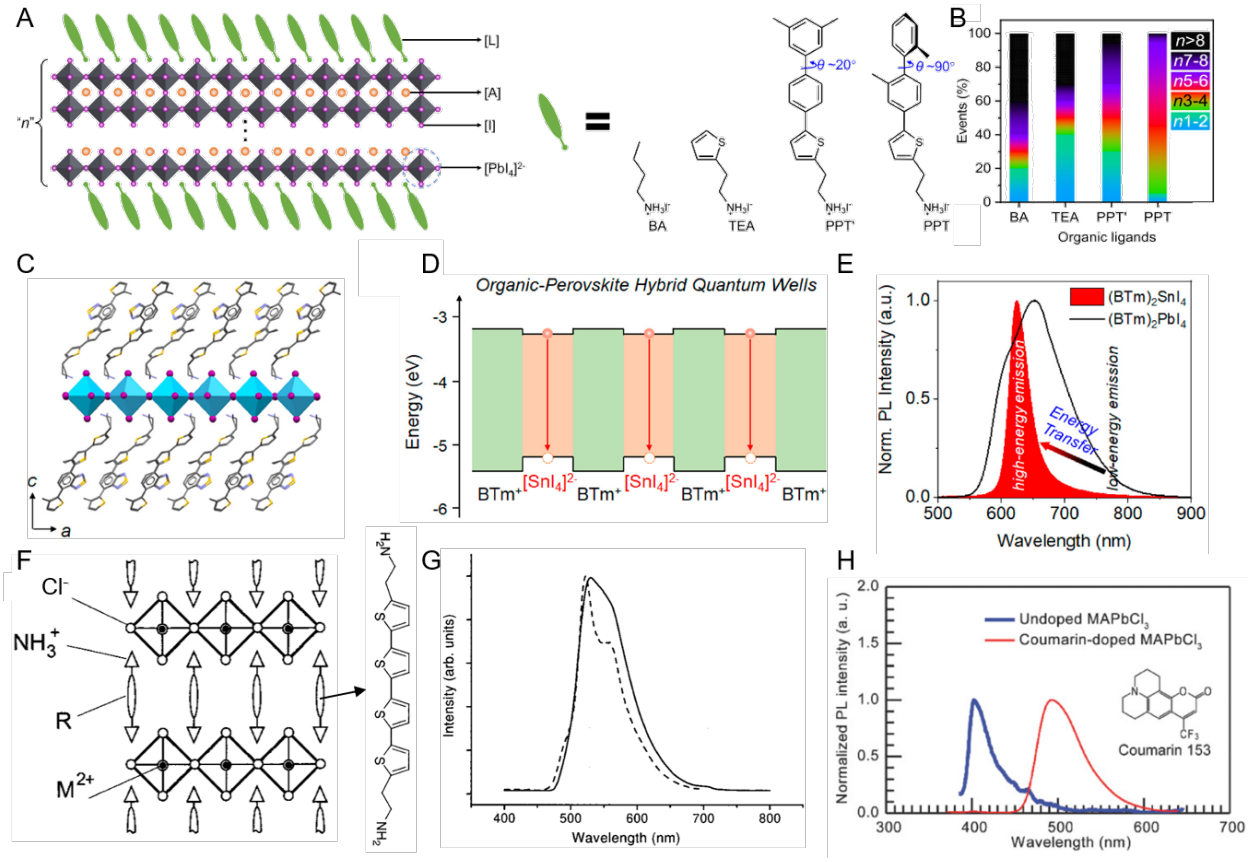

Figure 5. PeLEDs based on quasi-2D OSiPs. (A) Schematic diagram for "*n*" phase and molecular structures of four organic LA cations in quasi-2D perovskite with increasing bulkiness

from left to right; their capability to control *n* phase distribution and suppress high *n* phase perovskites after thermal annealing is characterized by absorption spectra and shown in (B).[80] (C) A scheme of 2D perovskite lattice using BTm as LA cations and (D) the formation of MQW structure with near-perfect Type-I band alignment.[27] (E) PL spectra of BTm_2SnI_4 and BTm_2PbI_4 are compared to demonstrate the efficient energy transfer in the former system. (F) Molecular structure of a diammonium quaterthiophene LA cation and the crystal structure of the perovskite formed. (G) Electroluminescence (EL, solid line) and PL spectra (dashed) of the perovskite formed using this quaterthiophene LA cations.[81] (H) PL spectra with and without an emissive organic molecule as the energy acceptor in a perovskite host.[82] (A-B) Reproduced with permission from ref 80. Copyright 2023 Springer Nature. (C-E) Reproduced with permission from ref 27. Copyright 2021 American Chemical Society. (F-G) Reproduced with permission from ref 81. Copyright 1999 American Chemical Society. (H) Reproduced with permission from ref 82. Copyright 2018 Wiley.

Finally, organic semiconducting LAs with tailored energy levels and band alignments can be used to improve charge transport and energy transfer in PeLEDs as demonstrated in the aforementioned Sn based PeLEDs using BTm as LAs. An EQE of 3.3% was achieved in *n*=1 PeLEDs owing to the near-perfect Type I alignment and efficient ET from BTm to the inorganic well (Figure 5C-E). (Figure 5E). Alternatively, the inverted Type-I alignment with inorganic metal-halides as energy donors also led to meaningful structures in 2D perovskite LED, which has been proposed decades ago in 1999 (Figure 5F-G).[81] In addition, instead of devising organic semiconducting cations, doping efficient organic emitters in a perovskite host can be developed to take advantages of OLEDs (Figure 5H), which could potentially expand the choices of organic semiconductor derivatives.[82]

Lasing from halide perovskites. Similar to 3D halide perovskites,[83–88] RP phase 2D perovskites are promising in the realm of nanolasers owing to their unique quantum well structures and enhanced environmental stability. In 1998, amplified spontaneous emission (ASE) was demonstrated for the first time with 2D perovskites, $(PEA)_2PbI_4$, at a cryogenic condition.[89] Since then, ASE or lasing behaviors have been achieved with solution-processed RP phase quasi-2D perovskite thin films or microstructures.[90–92] Nevertheless, multiple *n* phases with different bandgaps in the film inevitably resulted in cascaded exciton transfer from low *n* to high *n* species, where lasing emissions will eventually be originated from the high *n* species or even 3D components.[93]

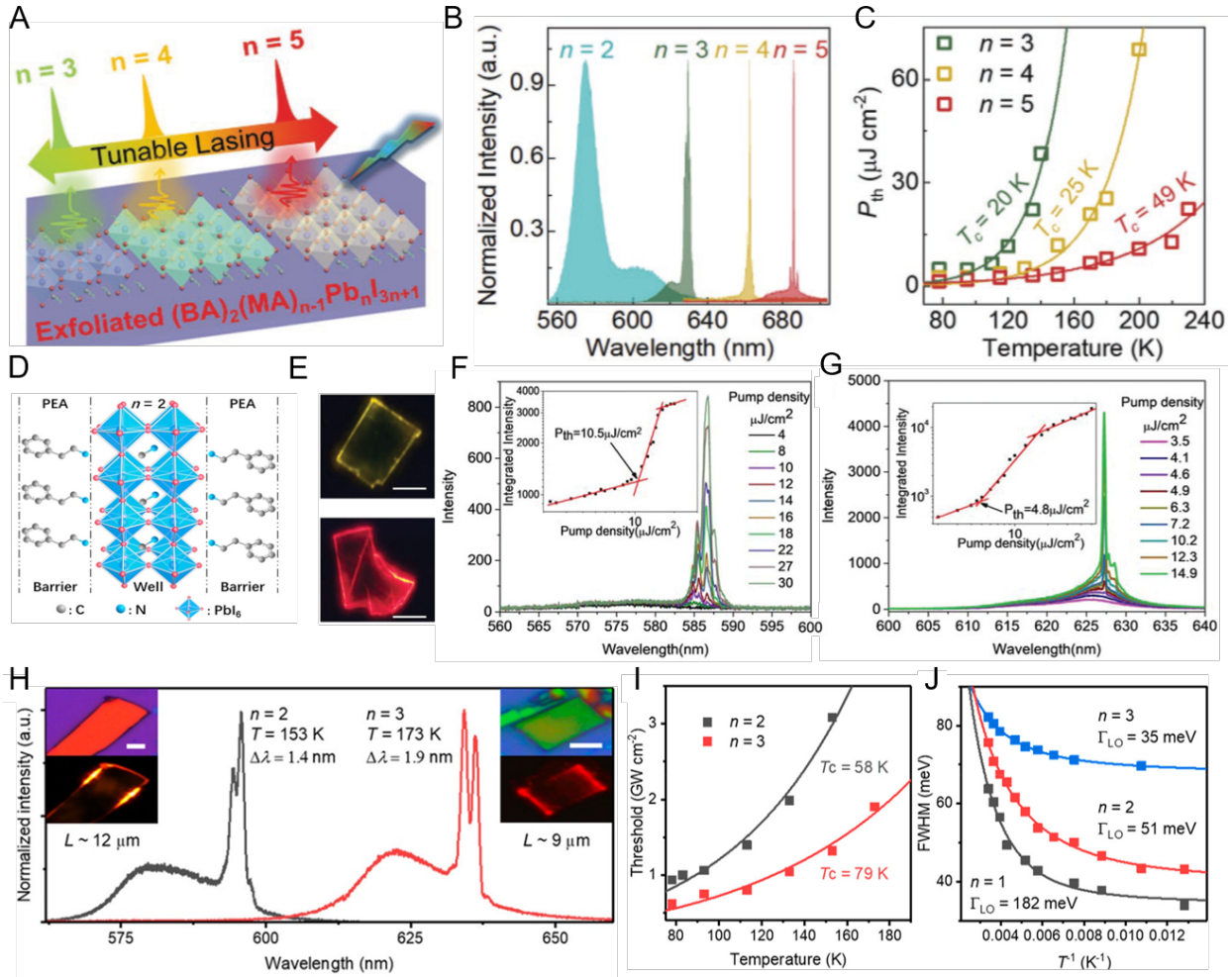

Figure 6. Lasing from exfoliated RPP crystals. (A) Schematic diagram of the RP perovskite lasers engineered by the inorganic well thickness.[94] (B) Lasing spectra of the RP perovskite microflakes for $n = 3$, 4, and 5 at 78 K. No lasing is observed from $n = 2$ species.[94] (C) Temperature dependence of lasing thresholds for n = 3, 4, and 5 perovskites.[94] (D) Schematic diagram of a $(PEA)_2(MA)_{n-1}Pb_nI_{3n+1}$ system ($n = 2$ as an example).[95] (E) The μ-PL pictures of RPPs with $n = 2$ (top), 3 (bottom) upon excitation by a 400 nm femtosecond laser above the lasing threshold at 20 K (scale bar 30 μm).[96] (F-G) μ-PL spectra and corresponding log–log plot of integrated emission intensity of an $n = 2$ (F) and 3 (G) RP perovskite flake as a function of pumped density P.[96] (H) Lasing spectra of perovskite flakes for $n = 2$ (left) and $n = 3$ (right) at 153 and 173 K, respectively (scale bar 5 μm).[95] (I) Lasing threshold as a function of temperature for $n = 2$ (black) and $n = 3$ (red) flakes. The characteristic temperatures (T_c) are fitted.[95] (J) The FWHM of spontaneous emission versus the inverse of temperature, $1/T$, for the perovskite flakes with $n = 1$, 2, and 3. The coupling strength of exciton-LO phonons (Γ_{LO}) is found to be 182, 51, and 35 meV for $n = 1$, 2, and 3 RPP flakes, respectively.[95] (A-C) Reproduced with permission from ref 94. Copyright 2019 Wiley. (D, H-J) Reproduced with permission from ref 95. Copyright 2022 American Chemical Society. (E-G) Reproduced with permission from ref 96. Copyright 2022 Wiley.

Recently, Liang *et al.*[94] reported efficient lasing from homologous RP phase 2D perovskites, $(BA)_2(MA)_{n-1}Pb_nI_{3n+1}$ single crystalline thin flakes (Figure 6A), with wavelengths ranging from 630 nm to 687 nm by increasing *n* from 3 to 5 (Figure 6B), respectively. Temperature dependent lasing characterizations reveal that the lasing threshold decreases exponentially as temperature decreases (Figure 6C), which can be well fitted by the equation: $P_{th} = P_{th,0}e^{T/T_c-1}$. This could be ascribed to the suppression of thermally-activated nonradiative processes. For a specific temperature, the lasing threshold also decreases as *n* number increases, which is interpreted as a result from reduced exciton-phonon interaction in a high *n*-phase crystal. It should be noted that no lasing is observed from $n \leq 2$ crystals even at a temperature as low as 78 K due to the stronger Auger recombination and exciton-phonon interaction in the lower-*n* 2D perovskites. Later, He *et al.*[96] replaced the above large organic spacer cations, BA, with PEA (Figure 6D) and demonstrated multiexciton lasing from $n = 3$ and even $n = 2$ single crystals at low temperatures (Figure 6E-G). Very recently, Gao *et al.*[95] further obtained two-photon pumped lasing emission from $(PEA)_2(MA)_{n-1}Pb_nI_{3n+1}$ single crystals with $n = 2$ and 3 (Figure 6H-J) under 800 nm laser excitation at low temperature (≤153 K). These results together suggest that bulky organic spacer cations play an important role in determining the lasing properties of single crystalline 2D perovskites.

Although impressive progress has been made in achieving lasing from 2D perovskites, almost all the measurements were carried out at low temperatures.[97] Based on previous reports, large organic spacer cations, for instance the bulky and organic semiconducting candidates, may be helpful to suppress exciton-phonon interactions or reduce Auger recombination.[78,98] This may lead to lasing from 2D perovskites at higher temperatures or even at room temperature. In addition, due to unique organic-inorganic quantum well structures of 2D perovskites, they are expected to allow lasing from the organic moieties with inversed type-I band alignment by engineering the energy level of organic and inorganic layers separately.[41] Moreover, considering the toxicity of lead element, further exploring Sn-based 2D perovskites for lasing application could also be an important subject.[27,99] As shown in more recent works,[100] this requires more delicate organic spacer cations design and fundamental insights of photophysics in 2D perovskites.

Summary and future implications

OSiPs as a new subclass of organic-inorganic hybrid metal-halide perovskites joins these next-generation materials with the long prosperous field of organic semiconductors, which emphasizes the exploitation on the organic-inorganic interfaces both from the design and tunability of inorganic metal-halides and organic cations. Tailor-designed organic semiconductors have been incorporated either on the surface of perovskites or as structure-directing cations, which has brought about considerable improvements on the stability and optoelectronic properties of these assembled systems as well as versatile novel interfacial band alignments and energy transfer mechanisms, inspiring the developments on futuristic light-emitting applications.

This perspective was initiated from an overview of recent OSiP systems and their advantages. The fundamental band alignment and energy transfer diagrams at the functional organic-inorganic interfaces were then organized based on the dissimilarities between organic and inorganic components. The inversed Type-I alignment featuring organic semiconductors as energy acceptors has been emphasized in this section with a special focus on harvesting the triplet excitons from organic semiconductors. Despite the fact that OSiPs have been demonstrated as advantageous matrices in this regard, current investigations haven't realized the full benefits of using perovskite matrices to enhance the emitting performances of organic semiconductors, especially triplet emitters. As the external heavy atom effects from lead-halide matrices could largely enhance the SOC efficiencies of organic cations, we anticipate that these hybrid systems could break the currently limited radiative recombination rate in organic triplet emitters. To further explore the inversed type I structure and the advantages of 2D perovskites as advanced matrices for organic semiconductors requires the design and incorporation of efficient organic phosphors or TADF molecules.

Our discussions were followed by exploring the recent PeLED and lasing applications of OSiPs, which have implied the need for organic semiconducting cations to provide additional stabilities and charge transport efficiencies in devices. While recent reports in quasi-2D PeLED systems have suggested promising advantages from using bulky semiconducting cations to suppress the phase segregation issue and achieve boosted operational stability, their potentials have not been well-elucidated in lasing systems or as passivators for 3D PeLEDs. On one hand, the versatile band-alignment from the wide tunability of organic semiconducting cations could allow lasing from the organic moieties with inversed type-I band alignment. On the other hand, contemporary explorations on small-molecule passivators have pointed out the significance of functional group

attachment to tune the surface vacancy formation energy, or the capabilities to extend the anchoring cation choices. These preliminary exploitations have called for the continuous search for organic semiconductors with sophisticated functionalities and adaptable structures that allow us to establish blueprints for OSiPs with the optimal combination of properties to fit various light-emitting applications.

AUTHOR INFORMATION

Corresponding Author

Letian Dou - Davidson School of Chemical Engineering, Purdue University, West Lafayette, IN, USA. E-mail: dou10@purdue.edu.

Notes

The authors declare no competing financial interests.

ACKNOWLEDGMENT

This work is supported by the US Department of Energy, Office of Basic Energy Sciences under award number DE-SC0022082 and US National Science Foundation under award number 2143568-DMR. The views expressed herein do not necessarily represent the views of the U.S. Department of Energy or the United States Government.

REFERENCES

(1) Xiao, Z.; Kerner, R. A.; Zhao, L.; Tran, N. L.; Lee, K. M.; Koh, T. W.; Scholes, G. D.; Rand, B. P. Efficient Perovskite Light-Emitting Diodes Featuring Nanometre-Sized Crystallites. *Nat Photonics* **2017**, *11* (2), 108–115.

(2) Zhao, B.; Lian, Y.; Cui, L.; Divitini, G.; Kusch, G.; Ruggeri, E.; Auras, F.; Li, W.; Yang, D.; Zhu, B.; et al. Efficient Light-Emitting Diodes from Mixed-Dimensional Perovskites on a Fluoride Interface. *Nat Electron* **2020**, *3* (11), 704–710.

(3) Wang, N.; Cheng, L.; Ge, R.; Zhang, S.; Miao, Y.; Zou, W.; Yi, C.; Sun, Y.; Cao, Y.; Yang, R.; et al. Perovskite Light-Emitting Diodes Based on Solution-Processed Self-Organized Multiple Quantum Wells. *Nat Photonics* **2016**, *10* (11), 699–704.

(4) Liu, Y.; Cui, J.; Du, K.; Tian, H.; He, Z.; Zhou, Q.; Yang, Z.; Deng, Y.; Chen, D.; Zuo, X.; et al. Efficient Blue Light-Emitting Diodes Based on Quantum-Confined Bromide Perovskite Nanostructures. *Nat Photonics* **2019**, *13* (11), 760–764.

(5) Jeong, M.; Choi, I. W.; Go, E. M.; Cho, Y.; Kim, M.; Lee, B.; Jeong, S.; Jo, Y.; Choi, H. W.; Lee, J.; et al. Stable Perovskite Solar Cells with Efficiency Exceeding 24.8% and 0.3-V Voltage Loss. *Science* **2020**, *369*, 1615-1620.

(6) Sahli, F.; Werner, J.; Kamino, B. A.; Bräuninger, M.; Monnard, R.; Paviet-Salomon, B.; Barraud, L.; Ding, L.; Diaz Leon, J. J.; Sacchetto, D.; et al. Fully Textured Monolithic Perovskite/Silicon Tandem Solar Cells with 25.2% Power Conversion Efficiency. *Nat Mater* **2018**, *17* (9), 820–826.

(7) Hao, F.; Stoumpos, C. C.; Cao, D. H.; Chang, R. P. H.; Kanatzidis, M. G. Lead-Free Solid-State Organic-Inorganic Halide Perovskite Solar Cells. *Nat Photonics* **2014**, *8* (6), 489–494.

(8) Dou, L.; Yang, Y. M.; You, J.; Hong, Z.; Chang, W. H.; Li, G.; Yang, Y. Solution-Processed Hybrid Perovskite Photodetectors with High Detectivity. *Nat Commun* **2014**, *5*, 5404.

(9) Yakunin, S.; Sytnyk, M.; Kriegner, D.; Shrestha, S.; Richter, M.; Matt, G. J.; Azimi, H.; Brabec, C. J.; Stangl, J.; Kovalenko, M. v.; et al. Detection of X-Ray Photons by Solution-Processed Lead Halide Perovskites. *Nat Photonics* **2015**, *9* (7), 444–449.

(10) Wei, H.; Fang, Y.; Mulligan, P.; Chuirazzi, W.; Fang, H. H.; Wang, C.; Ecker, B. R.; Gao, Y.; Loi, M. A.; Cao, L.; et al. Sensitive X-Ray Detectors Made of Methylammonium Lead Tribromide Perovskite Single Crystals. *Nat Photonics* **2016**, *10* (5), 333–339.

(11) Wei, H.; Desantis, D.; Wei, W.; Deng, Y.; Guo, D.; Savenije, T. J.; Cao, L.; Huang, J. Dopant Compensation in Alloyed CH3NH3PbBr3-x Clx Perovskite Single Crystals for Gamma-Ray Spectroscopy. *Nat Mater* **2017**, *16* (8), 826–833.

(12) Saparov, B.; Mitzi, D. B. Organic-Inorganic Perovskites: Structural Versatility for Functional Materials Design. *Chem Rev* **2016**, *116* (7), 4558–4596.

(13) Gao, Y.; Wei, Z.; Hsu, S. N.; Boudouris, B. W.; Dou, L. Two-Dimensional Halide Perovskites Featuring Semiconducting Organic Building Blocks. *Mater Chem Front* **2020**, *4* (12), 3400–3418.

(14) Gao, Y.; Dou, L. Organic Semiconductor-Incorporated Two-Dimensional Halide Perovskites. *Natl Sci Rev* **2022**, *9* (5), nwab111.

(15) Passarelli, J. v.; Fairfield, D. J.; Sather, N. A.; Hendricks, M. P.; Sai, H.; Stern, C. L.; Stupp, S. I. Enhanced Out-of-Plane Conductivity and Photovoltaic Performance in n = 1

Layered Perovskites through Organic Cation Design. *J Am Chem Soc* **2018**, *140* (23), 7313–7323.

(16) Ma, K.; Atapattu, H. R.; Zhao, Q.; Gao, Y.; Finkenauer, B. P.; Wang, K.; Chen, K.; Park, S. M.; Coffey, A. H.; Zhu, C.; et al. Multifunctional Conjugated Ligand Engineering for Stable and Efficient Perovskite Solar Cells. *Adv Mater* **2021**, *33*, 2100791.

(17) Mitzi, D. B.; Chondroudis, K.; Kagan, C. R. Design, Structure, and Optical Properties of Organic-Inorganic Perovskites Containing an Oligothiophene Chromophore. *Inorg Chem* **1999**, *38* (26), 6246–6256.

(18) Vickers, E. T.; Enlow, E. E.; Delmas, W. G.; Dibenedetto, A. C.; Chowdhury, A. H.; Bahrami, B.; Dreskin, B. W.; Graham, T. A.; Hernandez, I. N.; Carter, S. A.; et al. Enhancing Charge Carrier Delocalization in Perovskite Quantum Dot Solids with Energetically Aligned Conjugated Capping Ligands. *ACS Energy Lett* **2020**, *5* (3), 817–825.

(19) Philippe, B.; Park, B. W.; Lindblad, R.; Oscarsson, J.; Ahmadi, S.; Johansson, E. M. J.; Rensmo, H. Chemical and Electronic Structure Characterization of Lead Halide Perovskites and Stability Behavior under Different Exposures-A Photoelectron Spectroscopy Investigation. *Chem Mater* **2015**, *27* (5), 1720–1731.

(20) Quan, L. N.; Yuan, M.; Comin, R.; Voznyy, O.; Beauregard, E. M.; Hoogland, S.; Buin, A.; Kirmani, A. R.; Zhao, K.; Amassian, A.; et al. Ligand-Stabilized Reduced-Dimensionality Perovskites. *J Am Chem Soc* **2016**, *138* (8), 2649–2655.

(21) Leijtens, T.; Prasanna, R.; Gold-Parker, A.; Toney, M. F.; McGehee, M. D. Mechanism of Tin Oxidation and Stabilization by Lead Substitution in Tin Halide Perovskites. *ACS Energy Lett* **2017**, *2* (9), 2159–2165.

(22) Gu, F.; Zhao, Z.; Wang, C.; Rao, H.; Zhao, B.; Liu, Z.; Bian, Z.; Huang, C. Lead-Free Tin-Based Perovskite Solar Cells: Strategies Toward High Performance. *Solar RRL* **2019**, *3*, 1900213.

(23) Stoumpos, C. C.; Malliakas, C. D.; Kanatzidis, M. G. Semiconducting Tin and Lead Iodide Perovskites with Organic Cations: Phase Transitions, High Mobilities, and near-Infrared Photoluminescent Properties. *Inorg Chem* **2013**, *52* (15), 9019–9038.

(24) Chung, I.; Song, J. H.; Im, J.; Androulakis, J.; Malliakas, C. D.; Li, H.; Freeman, A. J.; Kenney, J. T.; Kanatzidis, M. G. CsSnI 3: Semiconductor or Metal? High Electrical Conductivity and Strong near-Infrared Photoluminescence from a Single Material. High Hole Mobility and Phase-Transitions. *J Am Chem Soc* **2012**, *134* (20), 8579–8587.

(25) Hsu, S. N.; Zhao, W.; Gao, Y.; Akriti; Segovia, M.; Xu, X.; Boudouris, B. W.; Dou, L. Thermoelectric Performance of Lead-Free Two-Dimensional Halide Perovskites Featuring Conjugated Ligands. *Nano Lett* **2021**, *21*, 7839–7844.

(26) Gao, Y.; Wei, Z.; Yoo, P.; Shi, E.; Zeller, M.; Zhu, C.; Liao, P.; Dou, L. Highly Stable Lead-Free Perovskite Field-Effect Transistors Incorporating Linear Π-Conjugated Organic Ligands. *J Am Chem Soc* **2019**, *141* (39), 15577–15585.

(27) Wang, K.; Jin, L.; Gao, Y.; Liang, A.; Finkenauer, B. P.; Zhao, W.; Wei, Z.; Zhu, C.; Guo, T. F.; Huang, L.; et al. Lead-Free Organic-Perovskite Hybrid Quantum Wells for Highly Stable Light-Emitting Diodes. *ACS Nano* **2021**, *15* (4), 6316–6325.

(28) Akriti; Lin, Z. Y.; Park, J. Y.; Yang, H.; Savoie, B. M.; Dou, L. Anion Diffusion in Two-Dimensional Halide Perovskites. *APL Mater* **2022**, *10*, 040903.

(29) Kim, H. S.; Jang, I. H.; Ahn, N.; Choi, M.; Guerrero, A.; Bisquert, J.; Park, N. G. Control of I-V Hysteresis in CH3NH3PbI3 Perovskite Solar Cell. *J Phys Chem Lett* **2015**, *6* (22), 4633–4639.

(30) Xiao, Z.; Yuan, Y.; Shao, Y.; Wang, Q.; Dong, Q.; Bi, C.; Sharma, P.; Gruverman, A.; Huang, J. Giant Switchable Photovoltaic Effect in Organometal Trihalide Perovskite Devices. *Nat Mater* **2015**, *14* (2), 193–197.

(31) Akriti; Zhang, S.; Lin, Z. Y.; Shi, E.; Finkenauer, B. P.; Gao, Y.; Pistone, A. J.; Ma, K.; Savoie, B. M.; Dou, L. Quantifying Anionic Diffusion in 2D Halide Perovskite Lateral Heterostructures. *Adv Mater* **2021**, *33*, 2105183.

(32) Roy, C. R.; Pan, D.; Wang, Y.; Hautzinger, M. P.; Zhao, Y.; Wright, J. C.; Zhu, Z.; Jin, S. Anion Exchange of Ruddlesden-Popper Lead Halide Perovskites Produces Stable Lateral Heterostructures. *J Am Chem Soc* **2021**, *143* (13), 5212–5221.

(33) Akriti; Shi, E.; Shiring, S. B.; Yang, J.; Atencio-Martinez, C. L.; Yuan, B.; Hu, X.; Gao, Y.; Finkenauer, B. P.; Pistone, A. J.; et al. Layer-by-Layer Anionic Diffusion in Two-Dimensional Halide Perovskite Vertical Heterostructures. *Nat Nanotechnol* **2021**, *16* (5), 584–591.

(34) Pan, D.; Fu, Y.; Spitha, N.; Zhao, Y.; Roy, C. R.; Morrow, D. J.; Kohler, D. D.; Wright, J. C.; Jin, S. Deterministic Fabrication of Arbitrary Vertical Heterostructures of Two-Dimensional Ruddlesden–Popper Halide Perovskites. *Nat Nanotechnol* **2021**, *16* (2), 159–165.

(35) Shi, E.; Dou, L. Halide Perovskite Epitaxial Heterostructures. *Acc Mater Res* **2020**, *1* (3), 213–224.

(36) Shi, E.; Yuan, B.; Shiring, S. B.; Gao, Y.; Akriti; Guo, Y.; Su, C.; Lai, M.; Yang, P.; Kong, J.; et al. Two-Dimensional Halide Perovskite Lateral Epitaxial Heterostructures. *Nature* **2020**, *580*, 614–620.

(37) Zhang, J.; Zhu, X.; Wang, M.; Hu, B. Establishing Charge-Transfer Excitons in 2D Perovskite Heterostructures. *Nat Commun* **2020**, *11*, 2618.

(38) Herz, L. M. Charge-Carrier Dynamics in Organic-Inorganic Metal Halide Perovskites. *Annu Rev Phys Chem* **2016**, *67*, 65–89.

(39) Straus, D. B.; Kagan, C. R. Electrons, Excitons, and Phonons in Two-Dimensional Hybrid Perovskites: Connecting Structural, Optical, and Electronic Properties. *J Phys Chem Lett* **2018**, *9* (6), 1434–1447.

(40) Knupfer, M. Exciton Binding Energies in Organic Semiconductors. *Appl Phys A Mater Sci Process* **2003**, *77* (5), 623–626.

(41) Gao, Y.; Shi, E.; Deng, S.; Shiring, S. B.; Snaider, J. M.; Liang, C.; Yuan, B.; Song, R.; Janke, S. M.; Liebman-Peláez, A.; et al. Molecular Engineering of Organic–Inorganic Hybrid Perovskites Quantum Wells. *Nat Chem* **2019**, *11* (12), 1151–1157.

(42) Guo, S.; Li, Y.; Mao, Y.; Tao, W.; Bu, K.; Fu, T.; Zhao, C.; Luo, H.; Hu, Q.; Zhu, H.; et al. Reconfiguring Band-Edge States and Charge Distribution of Organic Semiconductor-Incorporated 2D Perovskites via Pressure Gating. *Sci Adv* **2022**, *8*, eadd1984.

(43) Turro, N. J.; Ramamurthy, V.; Scaiano, J. C. Modern Molecular Photochemistry of Organic Molecules, First Indi. University Science Books: Sausalito, CA, 2012.

(44) Lédée, F.; Audebert, P.; Trippé-Allard, G.; Galmiche, L.; Garrot, D.; Marrot, J.; Lauret, J. S.; Deleporte, E.; Katan, C.; Even, J.; et al. Tetrazine Molecules as an Efficient Electronic Diversion Channel in 2D Organic-Inorganic Perovskites. *Mater Horiz* **2021**, *8* (5), 1547–1560.

(45) Fillafer, N.; Seewald, T.; Schmidt-Mende, L.; Polarz, S. Interfacial Charge Transfer Processes in 2D and 3D Semiconducting Hybrid Perovskites: Azobenzene as Photoswitchable Ligand. *Beilstein J Nanotechnol* **2020**, *11* (1), 466–479.

(46) Ema, K.; Inomata, M.; Kato, Y.; Kunugita, H.; Era, M. Nearly Perfect Triplet-Triplet Energy Transfer from Wannier Excitons to Naphthalene in Organic-Inorganic Hybrid Quantum-Well Materials. *Phys Rev Lett* **2008**, *100*, 257401.

(47) Era, M.; Maeda, K.; Tsutsui, T. Enhanced Phosphorescence from Naphthalene-Chromophore Incorporated into Lead Bromide-Based Layered Perovskite Having Organic-Inorganic Superlattice Structure. *Chem Phys Lett* **1998**, *296*, 417–420.

(48) Huang, Q.; Lin, Z.; Yan, D. Tuning Organic Room-Temperature Phosphorescence through the Confinement Effect of Inorganic Micro/Nanostructures. *Small Struct* **2021**, *2*, 2100044.

(49) Yang, S.; Wu, D.; Gong, W.; Huang, Q.; Zhen, H.; Ling, Q.; Lin, Z. Highly Efficient Room-Temperature Phosphorescence and Afterglow Luminescence from Common Organic Fluorophores in 2D Hybrid Perovskites. *Chem Sci* **2018**, *9* (48), 8975–8981.

(50) Hu, H.; Meier, F.; Zhao, D.; Abe, Y.; Gao, Y.; Chen, B.; Salim, T.; Chia, E. E. M.; Qiao, X.; Deibel, C.; et al. Efficient Room-Temperature Phosphorescence from Organic–Inorganic Hybrid Perovskites by Molecular Engineering. *Adv Mater* **2018**, *30*, 1707621.

(51) Hu, H.; Zhao, D.; Gao, Y.; Qiao, X.; Salim, T.; Chen, B.; Chia, E. E. M.; Grimsdale, A. C.; Lam, Y. M. Harvesting Triplet Excitons in Lead-Halide Perovskites for Room Temperature Phosphorescence. *Chem Mater* **2019**, *31* (7), 2597–2602.

(52) Shao, W.; Kim, J. Metal-Free Organic Phosphors toward Fast and Efficient Room-Temperature Phosphorescence. *Acc Chem Res* **2022**, *55* (11), 1573–1585.

(53) Yang, S.; Zhou, B.; Huang, Q.; Wang, S.; Zhen, H.; Yan, D.; Lin, Z.; Ling, Q. Highly Efficient Organic Afterglow from a 2D Layered Lead-Free Metal Halide in Both Crystals and Thin Films under an Air Atmosphere. *ACS Appl Mater Interfaces* **2020**, *12* (1), 1419–1426.

(54) Zhou, B.; Yan, D. Simultaneous Long-Persistent Blue Luminescence and High Quantum Yield within 2D Organic–Metal Halide Perovskite Micro/Nanosheets. *Angew Chem Int Ed* **2019**, *58* (42), 15128–15135.

(55) Murawski, C.; Leo, K.; Gather, M. C. Efficiency Roll-off in Organic Light-Emitting Diodes. *Adv Mater* **2013**, *25* (47), 6801–6827.

(56) Bolton, O.; Lee, K.; Kim, H. J.; Lin, K. Y.; Kim, J. Activating Efficient Phosphorescence from Purely Organic Materials by Crystal Design. *Nat Chem* **2011**, *3* (3), 205–210.

(57) Lee, D. R.; Lee, K. H.; Shao, W.; Kim, C. L.; Kim, J.; Lee, J. Y. Heavy Atom Effect of Selenium for Metal-Free Phosphorescent Light-Emitting Diodes. *Chem Mater* **2020**, *32* (6), 2583–2592.

(58) Shao, W.; Jiang, H.; Ansari, R.; Zimmerman, P. M.; Kim, J. Heavy Atom Oriented Orbital Angular Momentum Manipulation in Metal-Free Organic Phosphors. *Chem Sci* **2022**, *13* (3), 789–797.

(59) Uoyama, H.; Goushi, K.; Shizu, K.; Nomura, H.; Adachi, C. Highly Efficient Organic Light-Emitting Diodes from Delayed Fluorescence. *Nature* **2012**, *492*, 234–238.

(60) Wu, T. L.; Huang, M. J.; Lin, C. C.; Huang, P. Y.; Chou, T. Y.; Chen-Cheng, R. W.; Lin, H. W.; Liu, R. S.; Cheng, C. H. Diboron Compound-Based Organic Light-Emitting Diodes with High Efficiency and Reduced Efficiency Roll-Off. *Nat Photonics* **2018**, *12* (4), 235–240.

(61) Hu, Y. X.; Miao, J.; Hua, T.; Huang, Z.; Qi, Y.; Zou, Y.; Qiu, Y.; Xia, H.; Liu, H.; Cao, X.; et al. Efficient Selenium-Integrated TADF OLEDs with Reduced Roll-Off. *Nat Photonics* **2022**, *16* (11), 803–810.

(62) Kondo, Y.; Yoshiura, K.; Kitera, S.; Nishi, H.; Oda, S.; Gotoh, H.; Sasada, Y.; Yanai, M.; Hatakeyama, T. Narrowband Deep-Blue Organic Light-Emitting Diode Featuring an Organoboron-Based Emitter. *Nat Photonics* **2019**, *13* (10), 678–682.

(63) Zhao, L.; Rolston, N.; Lee, K. M.; Zhao, X.; Reyes-Martinez, M. A.; Tran, N. L.; Yeh, Y. W.; Yao, N.; Scholes, G. D.; Loo, Y. L.; et al. Influence of Bulky Organo-Ammonium Halide Additive Choice on the Flexibility and Efficiency of Perovskite Light-Emitting Devices. *Adv Funct Mater* **2018**, *28*, 1802060.

(64) Xiao, Z.; Kerner, R. A.; Tran, N.; Zhao, L.; Scholes, G. D.; Rand, B. P. Engineering Perovskite Nanocrystal Surface Termination for Light-Emitting Diodes with External Quantum Efficiency Exceeding 15%. *Adv Funct Mater* **2019**, *29*, 1807284.

(65) Fang, Z.; Chen, W.; Shi, Y.; Zhao, J.; Chu, S.; Zhang, J.; Xiao, Z. Dual Passivation of Perovskite Defects for Light-Emitting Diodes with External Quantum Efficiency Exceeding 20%. *Adv Funct Mater* **2020**, *30*, 1909754.

(66) Liang, A.; Wang, K.; Gao, Y.; Finkenauer, B. P.; Zhu, C.; Jin, L.; Huang, L.; Dou, L. Highly Efficient Halide Perovskite Light-Emitting Diodes via Molecular Passivation. *Angew Chem Int Ed* **2021**, *60* (15), 8337–8343.

(67) Zhao, B.; Bai, S.; Kim, V.; Lamboll, R.; Shivanna, R.; Auras, F.; Richter, J. M.; Yang, L.; Dai, L.; Alsari, M.; et al. High-Efficiency Perovskite–Polymer Bulk Heterostructure Light-Emitting Diodes. *Nat Photonics* **2018**, *12*, 783–789.

(68) Zou, W.; Li, R.; Zhang, S.; Liu, Y.; Wang, N.; Cao, Y.; Miao, Y.; Xu, M.; Guo, Q.; Di, D.; et al. Minimising Efficiency Roll-off in High-Brightness Perovskite Light-Emitting Diodes. *Nat Commun* **2018**, *9*, 608.

(69) Miao, Y.; Cheng, L.; Zou, W.; Gu, L.; Zhang, J.; Guo, Q.; Peng, Q.; Xu, M.; He, Y.; Zhang, S.; et al. Microcavity Top-Emission Perovskite Light-Emitting Diodes. *Light Sci Appl* **2020**, *9*, 89.

(70) Zhang, S.; Yi, C.; Wang, N.; Sun, Y.; Zou, W.; Wei, Y.; Cao, Y.; Miao, Y.; Li, R.; Yin, Y.; et al. Efficient Red Perovskite Light-Emitting Diodes Based on Solution-Processed Multiple Quantum Wells. *Adv Mater* **2017**, *29*, 1606600.

(71) Chang, J.; Zhang, S.; Wang, N.; Sun, Y.; Wei, Y.; Li, R.; Yi, C.; Wang, J.; Huang, W. Enhanced Performance of Red Perovskite Light-Emitting Diodes through the Dimensional Tailoring of Perovskite Multiple Quantum Wells. *J Phys Chem Lett* **2018**, *9* (4), 881–886.

(72) He, Z.; Liu, Y.; Yang, Z.; Li, J.; Cui, J.; Chen, D.; Fang, Z.; He, H.; Ye, Z.; Zhu, H.; et al. High-Efficiency Red Light-Emitting Diodes Based on Multiple Quantum Wells of Phenylbutylammonium-Cesium Lead Iodide Perovskites. *ACS Photonics* **2019**, *6* (3), 587–594.

(73) Meng, F.; Liu, X.; Chen, Y.; Cai, X.; Li, M.; Shi, T.; Chen, Z.; Chen, D.; Yip, H. L.; Ramanan, C.; et al. Co-Interlayer Engineering toward Efficient Green Quasi-Two-Dimensional Perovskite Light-Emitting Diodes. *Adv Funct Mater* **2020**, *30*, 1910167.

(74) Wang, K. H.; Peng, Y.; Ge, J.; Jiang, S.; Zhu, B. S.; Yao, J.; Yin, Y. C.; Yang, J. N.; Zhang, Q.; Yao, H. bin. Efficient and Color-Tunable Quasi-2D CsPbBr x Cl 3- x Perovskite Blue Light-Emitting Diodes. *ACS Photonics* **2019**, *6* (3), 667–676.

(75) Yantara, N.; Jamaludin, N. F.; Febriansyah, B.; Giovanni, D.; Bruno, A.; Soci, C.; Sum, T. C.; Mhaisalkar, S.; Mathews, N. Designing the Perovskite Structural Landscape for Efficient Blue Emission. *ACS Energy Lett* **2020**, *5* (5), 1593–1600.

(76) Cheng, L.; Cao, Y.; Ge, R.; Wei, Y. Q.; Wang, N. N.; Wang, J. P.; Huang, W. Sky-Blue Perovskite Light-Emitting Diodes Based on Quasi-Two-Dimensional Layered Perovskites. *Chin Chem Lett* **2017**, *28* (1), 29–31.

(77) Chen, Z.; Zhang, C.; Jiang, X. F.; Liu, M.; Xia, R.; Shi, T.; Chen, D.; Xue, Q.; Zhao, Y. J.; Su, S.; et al. High-Performance Color-Tunable Perovskite Light Emitting Devices through Structural Modulation from Bulk to Layered Film. *Adv Mater* **2017**, *29*, 1603157.

(78) Jiang, Y.; Cui, M.; Li, S.; Sun, C.; Huang, Y.; Wei, J.; Zhang, L.; Lv, M.; Qin, C.; Liu, Y.; et al. Reducing the Impact of Auger Recombination in Quasi-2D Perovskite Light-Emitting Diodes. *Nat Commun* **2021**, *12*, 336.

(79) Passarelli, J. v.; Mauck, C. M.; Winslow, S. W.; Perkinson, C. F.; Bard, J. C.; Sai, H.; Williams, K. W.; Narayanan, A.; Fairfield, D. J.; Hendricks, M. P.; et al. Tunable Exciton Binding Energy in 2D Hybrid Layered Perovskites through Donor–Acceptor Interactions within the Organic Layer. *Nat Chem* **2020**, *12* (8), 672–682.

(80) Wang, K.; Lin, Z.-Y.; Zhang, Z.; Jin, L.; Ma, K.; Coffey, A. H.; Atapattu, H. R.; Gao, Y.; Park, J. Y.; Wei, Z.; et al. Suppressing Phase Disproportionation in Quasi-2D Perovskite Light-Emitting Diodes. *Nat Commun* **2023**, *14*, 397.

(81) Chondroudis, K.; Mitzi, D. B. Electroluminescence from an Organic-Inorganic Perovskite Incorporating a Quaterthiophene Dye within Lead Halide Perovskite Layers. *Chem Mater* **1999**, *11* (11), 3028–3030.

(82) Matsushima, T.; Qin, C.; Goushi, K.; Bencheikh, F.; Komino, T.; Leyden, M.; Sandanayaka, A. S. D.; Adachi, C. Enhanced Electroluminescence from Organic Light-Emitting Diodes with an Organic–Inorganic Perovskite Host Layer. *Adv Mater* **2018**, *30*, 1802662.

(83) Xing, G.; Mathews, N.; Lim, S. S.; Yantara, N.; Liu, X.; Sabba, D.; Grätzel, M.; Mhaisalkar, S.; Sum, T. C. Low-Temperature Solution-Processed Wavelength-Tunable Perovskites for Lasing. *Nat Mater* **2014**, *13* (5), 476–480.

(84) Zhu, H.; Fu, Y.; Meng, F.; Wu, X.; Gong, Z.; Ding, Q.; Gustafsson, M. v.; Trinh, M. T.; Jin, S.; Zhu, X. Y. Lead Halide Perovskite Nanowire Lasers with Low Lasing Thresholds and High Quality Factors. *Nat Mater* **2015**, *14* (6), 636–642.

(85) Kondo, S.; Takahashi, K.; Nakanish, T.; Saito, T.; Asada, H.; Nakagawa, H. High Intensity Photoluminescence of Microcrystalline CsPbBr3 Films: Evidence for Enhanced Stimulated Emission at Room Temperature. *Curr Appl Phys* **2007**, *7* (1), 1–5.

(86) Wang, K.; Du, Y.; Liang, J.; Zhao, J.; Xu, F. F.; Liu, X.; Zhang, C.; Yan, Y.; Zhao, Y. S. Wettability-Guided Screen Printing of Perovskite Microlaser Arrays for Current-Driven Displays. *Adv Mater* **2020**, *32*, 2001999.

(87) Roh, K.; Zhao, L.; Gunnarsson, W. B.; Xiao, Z.; Jia, Y.; Giebink, N. C.; Rand, B. P. Widely Tunable, Room Temperature, Single-Mode Lasing Operation from Mixed-Halide Perovskite Thin Films. *ACS Photonics* **2019**, *6* (12), 3331–3337.

(88) Zhizhchenko, A.; Syubaev, S.; Berestennikov, A.; Yulin, A. v.; Porfirev, A.; Pushkarev, A.; Shishkin, I.; Golokhvast, K.; Bogdanov, A. A.; Zakhidov, A. A.; et al. Single-Mode Lasing from Imprinted Halide-Perovskite Microdisks. *ACS Nano* **2019**, *13* (4), 4140–4147.

(89) Kondo, T.; Azuma, T.; Yuasa, T.; Ito, R. Biexciton Lasing in the Layered Perovskite-Type Material (C6H13NH3)2PbI4. *Solid State Commun* **1998**, *105* (4), 253–255.

(90) Qin, C.; Sandanayaka, A. S. D.; Zhao, C.; Matsushima, T.; Zhang, D.; Fujihara, T.; Adachi, C. Stable Room-Temperature Continuous-Wave Lasing in Quasi-2D Perovskite Films. *Nature* **2020**, *585*, 53–57.

(91) Li, M.; Wei, Q.; Muduli, S. K.; Yantara, N.; Xu, Q.; Mathews, N.; Mhaisalkar, S. G.; Xing, G.; Sum, T. C. Enhanced Exciton and Photon Confinement in Ruddlesden–Popper Perovskite Microplatelets for Highly Stable Low-Threshold Polarized Lasing. *Adv Mater* **2018**, *30*, 1707235.

(92) Zhang, H.; Liao, Q.; Wu, Y.; Zhang, Z.; Gao, Q.; Liu, P.; Li, M.; Yao, J.; Fu, H. 2D Ruddlesden–Popper Perovskites Microring Laser Array. *Adv Mater* **2018**, *30*, 1706186.

(93) Wang, K.; Park, J. Y.; Akriti; Dou, L. Two-dimensional Halide Perovskite Quantum-well Emitters: A Critical Review. *EcoMat* **2021**, *3*, e12104.

(94) Liang, Y.; Shang, Q.; Wei, Q.; Zhao, L.; Liu, Z.; Shi, J.; Zhong, Y.; Chen, J.; Gao, Y.; Li, M.; et al. Lasing from Mechanically Exfoliated 2D Homologous Ruddlesden–Popper Perovskite Engineered by Inorganic Layer Thickness. *Adv Mater* **2019**, *31*, 1903030.

(95) Gao, W.; Wei, Q.; Wang, T.; Xu, J.; Zhuang, L.; Li, M.; Yao, K.; Yu, S. F. Two-Photon Lasing from Two-Dimensional Homologous Ruddlesden-Popper Perovskite with Giant Nonlinear Absorption and Natural Microcavities. *ACS Nano* **2022**, *16* (8), 13082-13091.

(96) He, X.; Gong, H.; Huang, H.; Li, Y.; Ren, J.; Li, Y.; Liao, Q.; Gao, T.; Fu, H. Multicolor Biexciton Lasers Based on 2D Perovskite Single Crystalline Flakes. *Adv Opt Mater* **2022**, *10*, 2200238.

(97) Raghavan, C. M.; Chen, T. P.; Li, S. S.; Chen, W. L.; Lo, C. Y.; Liao, Y. M.; Haider, G.; Lin, C. C.; Chen, C. C.; Sankar, R.; et al. Low-Threshold Lasing from 2D Homologous Organic-Inorganic Hybrid Ruddlesden-Popper Perovskite Single Crystals. *Nano Lett* **2018**, *18* (5), 3221–3228.

(98) Gong, X.; Voznyy, O.; Jain, A.; Liu, W.; Sabatini, R.; Piontkowski, Z.; Walters, G.; Bappi, G.; Nokhrin, S.; Bushuyev, O.; et al. Electron-Phonon Interaction in Efficient Perovskite Blue Emitters. *Nat Mater* **2018**, *17* (6), 550–556.

(99) Liang, A.; Gao, Y.; Asadpour, R.; Wei, Z.; Finkenauer, B. P.; Jin, L.; Yang, J.; Wang, K.; Chen, K.; Liao, P.; et al. Ligand-Driven Grain Engineering of High Mobility Two-Dimensional Perovskite Thin-Film Transistors. *J Am Chem Soc* **2021**, *143* (37), 15215–15223.

(100) Alvarado-Leaños, A. L.; Cortecchia, D.; Saggau, C. N.; Martani, S.; Folpini, G.; Feltri, E.; Albaqami, M. D.; Ma, L.; Petrozza, A. Lasing in Two-Dimensional Tin Perovskites. *ACS Nano* **2022**.